Multiple channels for horizontal, but only one for vertical corrugations? A new look at the stereo anisotropy

Ignacio Serrano-Pedraza
Institute of Neuroscience, Newcastle University, Newcastle upon Tyne, UK

Jenny C. A. Read
Institute of Neuroscience, Newcastle University, Newcastle upon Tyne, UK

Stereo vision displays a well-known anisotropy: disparity-defined slant is easier to detect for rotations about a horizontal axis than about a vertical axis, and low-frequency sinusoidal depth corrugations are easier to detect when the corrugations are horizontal than when they are vertical. Here, we determined disparity thresholds for vertically and horizontally oriented depth corrugations with both sinusoidal and square-wave profiles. We found that the orientation anisotropy for square waves is much weaker than for sine waves and is almost independent of frequency. This weaker anisotropy for square waves can be explained by considering the Fourier harmonics present in the stimulus. Using linear models imported from the luminance and texture perception domain, the disparity thresholds for square waves can be very well predicted from those for sine waves, for both horizontally and vertically oriented corrugations. For horizontally oriented corrugations, models based on the root mean square of the output of a single linear channel or the output of multiple linear channels worked equally well. This is consistent with previous evidence suggesting that stereo vision has multiple channels tuned to different spatial frequencies of horizontally oriented disparity modulations. However, for vertically oriented corrugations, only the root mean squared output of a single linear channel explained the data. We suggest that the stereo anisotropy may arise because the stereo system possesses multiple spatial frequency channels for detecting horizontally oriented modulations in horizontal disparity, but only one for vertically oriented modulations.

Keywords: binocular vision, disparity sensitivity function, orientation stereo anisotropy, linear stereo mechanisms

Citation: Serrano-Pedraza, I., & Read, J. C. A. (2010). Multiple channels for horizontal, but only one for vertical corrugations? A new look at the stereo anisotropy. *Journal of Vision, 10*(12):10, 1–11, http://www.journalofvision.org/content/10/12/10, doi:10.1167/10.12.10.

Introduction

Just as luminance gratings have been widely used to probe information processing within the visual system, disparity gratings or depth corrugations have been used to probe stereo vision. For example, Rogers and Graham (1982) and Tyler (1974) examined the disparity sensitivity function, the analogue of the contrast sensitivity function in the luminance domain. Disparity sensitivity is the reciprocal of disparity threshold, which is the minimum disparity amplitude needed to detect a corrugation with 85% accuracy. The maximum sensitivity (lowest disparity threshold) of the human visual system occurs between 0.2 and 0.6 cycle/deg; outside this range there is a fall-off in sensitivity for both lower and higher spatial frequencies (Bradshaw & Rogers, 1999; Rogers & Graham, 1982; Tyler, 1991). Thus, the disparity sensitivity function has an inverted U-shape similar to that found with luminance gratings (Campbell & Robson, 1968), possibly because the same type of operations are involved in detecting both disparity corrugations and luminance modulations. For example, lateral inhibition may reduce the sensitivity to sinusoidal corrugations of low spatial frequencies (Tyler, 1991).

The preeminence of sine-wave gratings in the luminance domain stems from Campbell and Robson's groundbreaking demonstration that the visibility of luminance gratings with different profiles—e.g., square wave or sawtooth—can be predicted from the contrast sensitivity function obtained with sine gratings. The different Fourier components combine almost linearly, suggesting that the visual system analyzes luminance within independent linear channels tuned to a limited range of spatial frequency and orientation. Accordingly, almost all studies of disparity corrugations have used gratings with a sine-wave depth profile. Yet the evidence that linear systems theory holds in the stereo domain is much less secure than for luminance. Masking and adaptation results suggest that stereo vision does contain multiple channels tuned to the spatial frequency of disparity modulation (Schumer & Ganz, 1979), but that these have much wider bandwidth than in the luminance domain. Furthermore, the percept caused by gratings whose frequency is too high to be detected suggests an important qualitative difference between the encoding of disparity and that of luminance. High-frequency, high-contrast luminance gratings appear as a uniform gray equal to the average luminance of the black and white stripes. Yet high-frequency, large-amplitude disparity corrugations can readily be distinguished

doi: 10.1167/10.12.10 Received July 19, 2010; published October 12, 2010 ISSN 1534-7362 © ARVO

Downloaded From: http://jov.arvojournals.org/pdfaccess.ashx?url=/data/Journals/JOV/933485/ on 04/12/2016

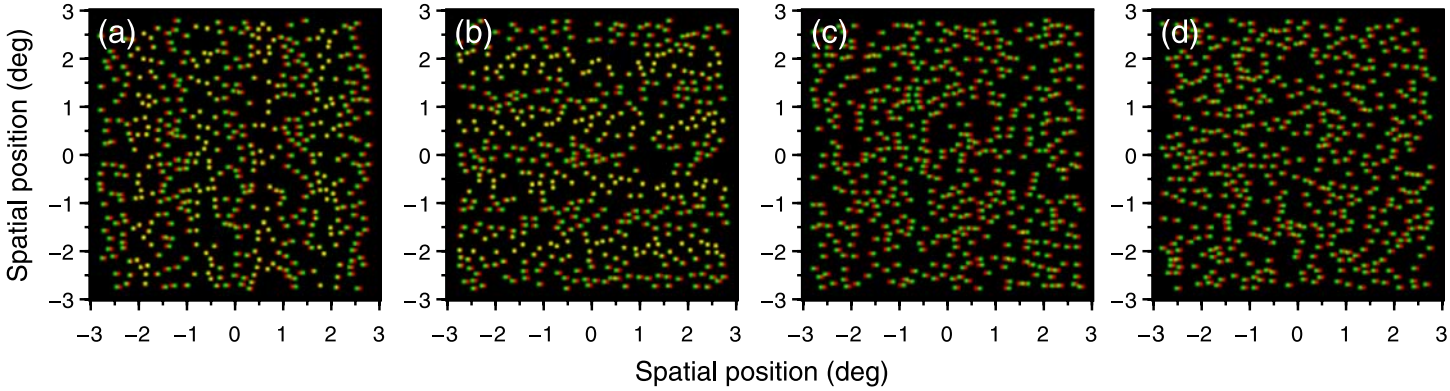

Figure 1. Anaglyph samples of random Gaussian dot stereograms used in the experiments. (a) Example of a stimulus with vertical sinusoidal wave corrugations defined by horizontal disparities. (b) Horizontal sinusoidal wave corrugations. (c) Vertical square-wave corrugations. (d) Horizontal square-wave corrugations. Spatial frequency: 0.4 cycle/deg. The sketches representing the 3D percept produced by these stimuli are represented in Figure 2a. (Note that the real stimuli were presented in a window of 12° × 12° and were perceived through polarizing filters.)

from a flat surface with uniform disparity equal to the average disparity of the near and far stripes. Rather, the percept is of a thickened surface, with elements at all disparities present in the grating.

In this paper, we measure disparity thresholds for horizontally and vertically oriented square-wave disparity corrugations (see Figures 1c and 1d). If the linear system analysis pioneered by Campbell and Robson in the luminance domain also holds for disparity, we should be able to predict the thresholds for these two stimuli from the thresholds measured with sine-wave corrugations. This is a particularly interesting stimulus to study, since stereo vision displays a striking orientation anisotropy that has no counterpart in the luminance domain. Sinusoidal disparity corrugations at low spatial frequencies are much easier to detect when the corrugations are horizontally oriented than when they are vertically oriented (Bradshaw, Hibbard, Parton, Rose, & Langley, 2006; Bradshaw & Rogers, 1999; van der Willigen, Harmening, Vossen, & Wagner, 2010). No one has yet examined whether this anisotropy holds for square-wave corrugations.

Methods

Subjects

We obtained data from a total of 5 human subjects; 2 authors (ISP, JCAR) and 3 observers unaware of the purpose of the study, all of them with experience in psychophysical observation (in total, 4 males, 1 female, aged between 18 and 37 years). All subjects had normal or corrected-to-normal refraction and normal visual acuity. Experimental procedures were approved by Newcastle University's Faculty of Medical Sciences Ethics Committee.

Equipment

The experiments were carried out in a dark room. Stimuli were presented on a rear projection screen (300 × 200 cm, Stewart Filmscreen 150, www.stewartfilm.com, supplied by Virtalis, Manchester), frontoparallel to the observers, who viewed it from a distance of 120 cm. A chin rest (UHCOTech HeadSpot) was used to stabilize the subject's head and to control the observation distance. Each eye's image was presented using a separate F2x+ Digital Light Processing projector (ProjectionDesign, Gamle Fredrikstad, Norway; www.projectiondesign.com) driven by an NVIDIA GeForce 8600 GT graphics card, with a spatial resolution of 1400 × 1050 pixels (horizontal × vertical) and a temporal resolution of 60 Hz. Both displays were gamma corrected using a Minolta LS-100 photometer. Polarizing filters ensured that each eye saw only one projector's image; the interocular cross-talk was less than 2%. The images were carefully aligned to within a pixel everywhere within the central 30° to ensure that as far as possible the only disparities were those introduced by the experimenter (Serrano-Pedraza & Read, 2009b). The projected image was 71 × 53 cm subtending 33° × 25°. Each pixel thus subtended 1.41 minutes of arc (arcmin). The stimuli occupied the central 500×500 pixels (12° × 12°). All experiments were controlled by a DELL workstation running MATLAB 7.5 (R2007b) with the Psychophysics Toolbox extensions (Brainard, 1997, Pelli, 1997, www.psychtoolbox.org).

White on our display had a luminance of 4 cd/m^2 and reduced to 2.8 cd/m^2 when viewed through the polarizing glasses; the black background had a luminance of 0.07 cd/m^2 and reduced to 0.05 cd/m^2.

Downloaded From: http://jov.arvojournals.org/pdfaccess.ashx?url=/data/Journals/JOV/933485/ on 04/12/2016

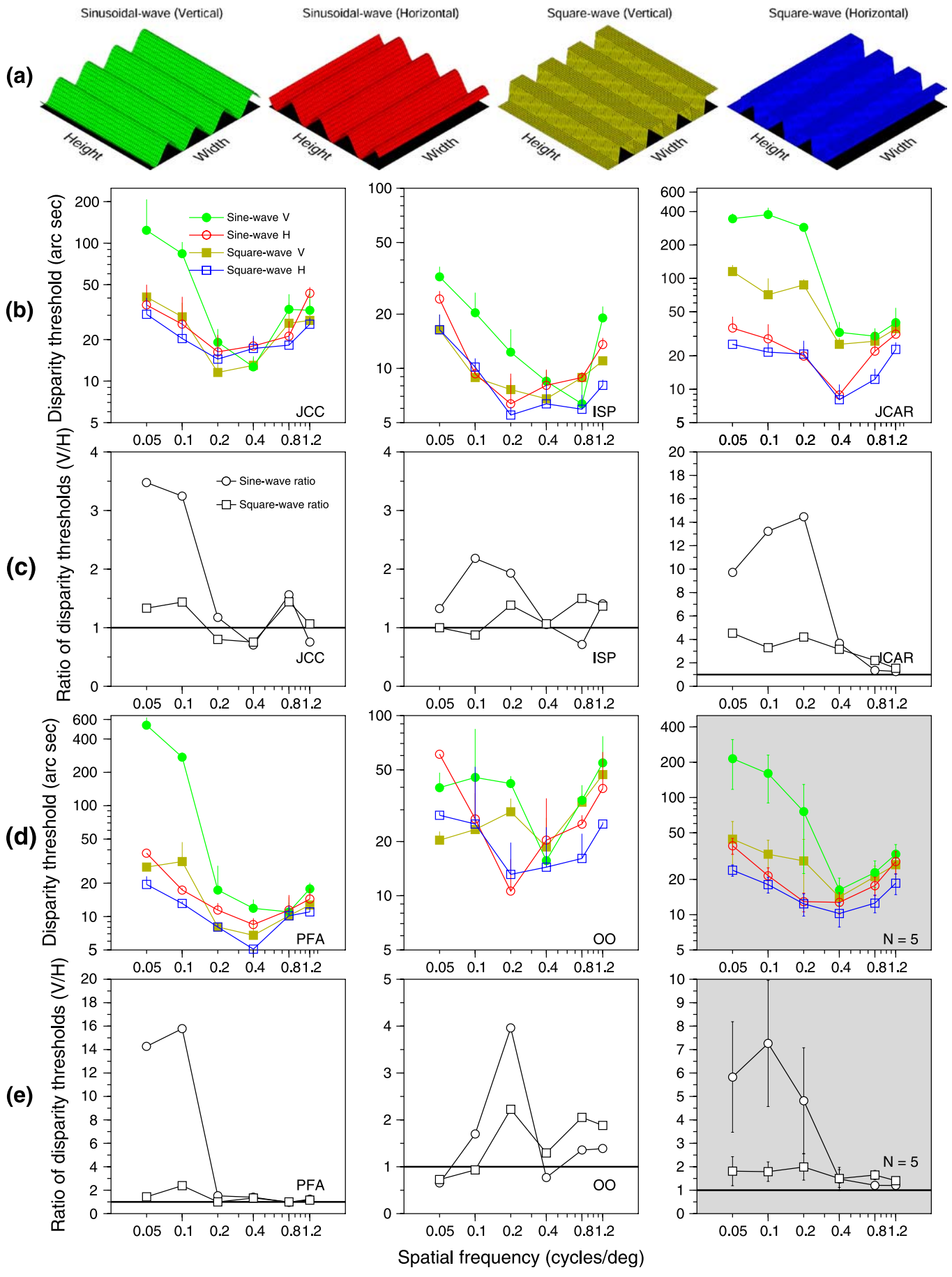

Downloaded From: http://jov.arvojournals.org/pdfaccess.ashx?url=/data/Journals/JOV/933485/ on 04/12/2016

Stimulus generation

All stimuli were random-dot stereograms consisting of white dots on a black background. The dots were isotropic two-dimensional Gaussians with a standard deviation of $\sigma_{dot} = 1.44$ arcmin (the dots had a dimension of 5 × 5 pixels). Dots were scattered randomly but without overlap. The luminance of each pixel was calculated according to the value of the Gaussian function at the center of the pixel, thus allowing subpixel disparities. Dot density was $\rho = 14.08$ dots/deg^2, giving a Nyquist limit of $f_N = 1.87$ cycles/deg ($f_N = 0.5\sqrt{\rho}$; see Figure 1).

Each dot was given a horizontal disparity δ on the screen, according to the desired waveform, e.g., $\delta = \pm A/2\cos(2\pi fy)$ for a horizontally oriented sine wave; $\delta = \pm A/2\mathrm{sgn}(\cos(2\pi fx))$ for a vertically oriented square wave, where $A/2$ is the disparity amplitude of the grating and f is its spatial frequency. Dots were given uniform disparity and remained circular even when depicted as lying on the sloping regions of sine-wave corrugations. The dot size was much less than the shortest spatial period used (50 arcmin), and disparity amplitudes were small; as we shall see in the Results (Figure 2), the maximum value of fA was 0.02 while the maximum f was 1.2 cpd. Thus, the disparity change that should have occurred across a dot, $2\pi\sigma_{dot}fA$, never exceeded 0.15 arcmin or 11% of the grating amplitude.

There are intrinsic problems with using horizontal disparity to depict vertically oriented depth corrugations. First, such corrugations necessarily include variations in dot density, which could provide a monocular cue to depth. In practice, these are only visible for disparity amplitudes well above threshold (Bradshaw & Rogers, 1999, Tyler & Raibert, 1975), and in any case cannot explain why performance is *worse* on vertically oriented gratings.

For vertically oriented gratings, the period of the stimulus imposes an upper limit on the disparity range. Because our experiments measured thresholds and thus used very small disparities, we do not approach this limit.

Additionally, for vertically oriented square-wave gratings, one has to decide whether to depict dots on transparent or opaque surfaces. To depict an opaque black surface, one must remove dots at the edges of the far slats, which are hidden from view by the near slats. We did not do this, thus depicting dots lying on a transparent surface.

Both the previous points depend on the ratio between the disparity amplitude and the half-period of the grating: fA, which in our stimuli does not exceed 0.02. This means that the disparity amplitude is much less than the upper limit, and the distinction between opaque and transparent surfaces is negligible (because areas that would have been occluded by an opaque surface form a tiny fraction of the stimulus).

Procedure

In this experiment, we compared two depth corrugations (sinusoidal vs. square wave) defined by horizontal disparity. Corrugations had two possible orientations (vertical vs. horizontal) and six corrugation frequencies (0.05, 0.1, 0.2, 0.4, 0.8, and 1.2 cycles/deg) with phase 0 rad (see examples of the stimuli in Figure 1). The random-dot stimuli were 12° × 12° (500 × 500 pixels). To obtain the lowest spatial frequency, 0.05 cycle/deg, we used the same on-screen stimulus as for 0.1 cycle/deg but reduced the distance to the screen from 120 cm to 60 cm.

Peak-to-trough amplitude disparity thresholds were measured using adaptive Bayesian staircases (Treutwein, 1995) in a two-interval forced-choice task where random dots were presented with zero disparity in one presentation interval and with corrugation in the other. The task was to indicate the interval containing the disparity corrugation.

A different uniform random distribution of dots was presented in each interval. Corrugation spatial frequencies were blocked, but orientations and type of wave modulations (sinusoidal or square wave) were interleaved.

To minimize vergence movements, the subjects were instructed to maintain fixation on a small cross (0.3° × 0.3°) in the center of the screen, flanked by vertical and horizontal Nonius lines of length 0.6°, presented in between stimuli. Each presentation interval was preceded by these Nonius lines presented for 300 ms followed by 200 ms of a blank screen. The presentation intervals lasted 250 ms, so the total trial duration was 1500 ms (Nonius lines + blank + first interval + Nonius lines + blank + second interval). A new trial was initiated after the participant's response, thus the experiments proceeded at a pace determined by the observer. In general, between 6 and 8 min were required per disparity threshold estimation. No feedback about correctness on individual trials was given.

The characteristics of the Bayesian staircases were: (1) the prior probability density function was uniform (Emerson, 1986; Pentland, 1980); (2) the model likelihood function was the logistic function adapted from García-Pérez (1998, Appendix A) with a spread value of 0.8 (with delta parameter equal to 0.01), a lapse rate of

Figure 2. Disparity thresholds for five subjects, i.e., peak-to-trough range of the disparity corrugation at which performance was 85% correct. (a) Sketches representing the 3D percept produced by sinusoidal and square corrugation with horizontal and vertical orientations. Color of the sketches matches the corresponding results in the panels. (b, d) Mean + *SD* of disparity thresholds (arc sec) as a function of the spatial frequency (cycles/deg) of the corrugations. (c, e) Ratio between disparity thresholds with the same corrugations but different orientations (vertical divided by horizontal) as a function of the spatial frequency. The ratio value of 1 corresponds to identical disparity thresholds, and values greater than 1 correspond to higher threshold (lower sensitivity) to detect the vertical corrugations. The rightmost panels with gray background in (d) and (e) show the mean ± *SEM* of all subjects.

Downloaded From: http://jov.arvojournals.org/pdfaccess.ashx?url=/data/Journals/JOV/933485/ on 04/12/2016

0.01, and a guess rate of 0.5; (3) the value of the disparity in each trial was obtained from the mean of the posterior probability distribution (King-Smith, Grigsby, Vingrys, Benes, & Supowit, 1994); (4) the staircase stopped after 50 trials (Anderson, 2003; Pentland, 1980); and (5) the final threshold was estimated from the mean of the final probability density function. The disparity threshold corresponded to the value 0.85 of the subject's psychometric function. Two threshold estimations per condition were obtained for each subject. A total of 24 conditions (6 corrugation frequencies × 2 waveforms × 2 orientations) were tested over several experimental sessions.

Results

We examined two corrugation waveforms (sinusoidal and square wave) at two orientations (vertical and horizontal; see sample stimuli in Figure 1). Figure 2 shows the results for five subjects. Figures 2b and 2d show the disparity thresholds (i.e., the minimum peak-to-trough amplitude disparity needed for 85% correct performance) for four stimuli as a function of the spatial frequency of the corrugation.

Open and filled circles show the data for sinusoidal wave corrugations; green filled circles for vertical orientation and red open circles for horizontal orientation. Open and filled squares show the data for square-wave corrugations; brown filled squares for vertically oriented corrugations and blue open squares for horizontal.

Disparity thresholds for all 4 corrugation stimuli show the classical U-shape (Bradshaw & Rogers, 1999; Rogers & Graham, 1982; van der Willigen et al., 2010), with a fall-off in sensitivity for low and high frequencies similar to that found in the luminance domain (Campbell & Robson, 1968). From the average data (Figure 2d, rightmost panel), the minimum disparity threshold (maximum sensitivity) in all conditions was found for a corrugation frequency about 0.4 cycle/deg, in agreement with previous reports (Bradshaw & Rogers, 1999; Rogers & Graham, 1982; Tyler, 1991).

The data in Figure 2 exemplify the well-known stereo anisotropy for sinusoidal disparity corrugations. At frequencies below about 0.4 cycle/deg, disparity thresholds are much lower for horizontal sinusoidal corrugations (green filled circles) than for vertical sinusoidal corrugations (red open circles; Bradshaw et al., 2006; Bradshaw & Rogers, 1999; van der Willigen et al., 2010).

Figures 2c and 2e plot the ratio of the threshold for vertical corrugations to that for horizontal corrugations. Values greater than 1 indicate an anisotropy such that sensitivity is greater for horizontal corrugations. All subjects show this anisotropy for sinusoidal corrugations with spatial frequencies <0.4 cycle/deg; for subjects ISP and OO, this anisotropy disappears again at the lowest spatial frequency tested. Averaged over all 5 subjects, vertical sinusoidal corrugations of 0.1 cycle/deg require seven times the amplitude to be detected, compared to horizontal corrugations. At high frequencies, the anisotropy virtually disappears.

In contrast, for square-wave corrugations, the anisotropy is much weaker (threshold ratio of 1.5–2.5) and is almost independent of spatial frequency. Horizontally oriented square- and sine-wave corrugations have similar thresholds (slightly lower for square wave); vertically oriented square-wave corrugations are slightly harder again, whereas vertically oriented sine-wave corrugations are much more difficult still.

Linear system analysis

To explore whether these results can be explained with a linear system analysis, we examine three common linear models used in luminance and in texture perception (Campbell & Robson, 1968; Kingdom & Keeble, 1996), summarized in Figure 3. In this section, we will explain how the disparity threshold for square-wave corrugations can be predicted from the thresholds measured for sine-wave corrugations (with the same orientation), for each of the three models.

Peak detector single-channel model (peak)

This model assumes that the signal is detected by a single channel. The input waveform is filtered through this channel, and the output waveform is detected if its peak exceeds some threshold. In this model, the filter applied by this channel can be read out from the disparity sensitivity function DSF(ν), the inverse of the peak-to-trough disparity threshold function obtained with sinusoidal corrugations (see Figures 2 and 6). Thus, to predict the threshold with this model, we first multiply the Fourier transform of the signal by the disparity sensitivity function, then take the inverse Fourier transform and finally calculate the peak value of the output signal (Campbell & Robson, 1968, their Figure 3).

The peak of the output waveform for a square-wave corrugation with peak-to-trough amplitude A_{sq} is

$$P = A_{sq}\max\left[\frac{4}{\pi}\sum_{n=1,3,5\ldots}^{\infty}\frac{\mathrm{DSF}(nf_1)}{n}\sin(2\pi nf_1 x)\right], \qquad (1)$$

where f_1 is the spatial frequency of the fundamental or first harmonic.

We used linear interpolation to estimate the DSF at the spatial frequencies where we do not have data. We have not normalized the filter, since this will cancel out below.

Downloaded From: http://jov.arvojournals.org/pdfaccess.ashx?url=/data/Journals/JOV/933485/ on 04/12/2016

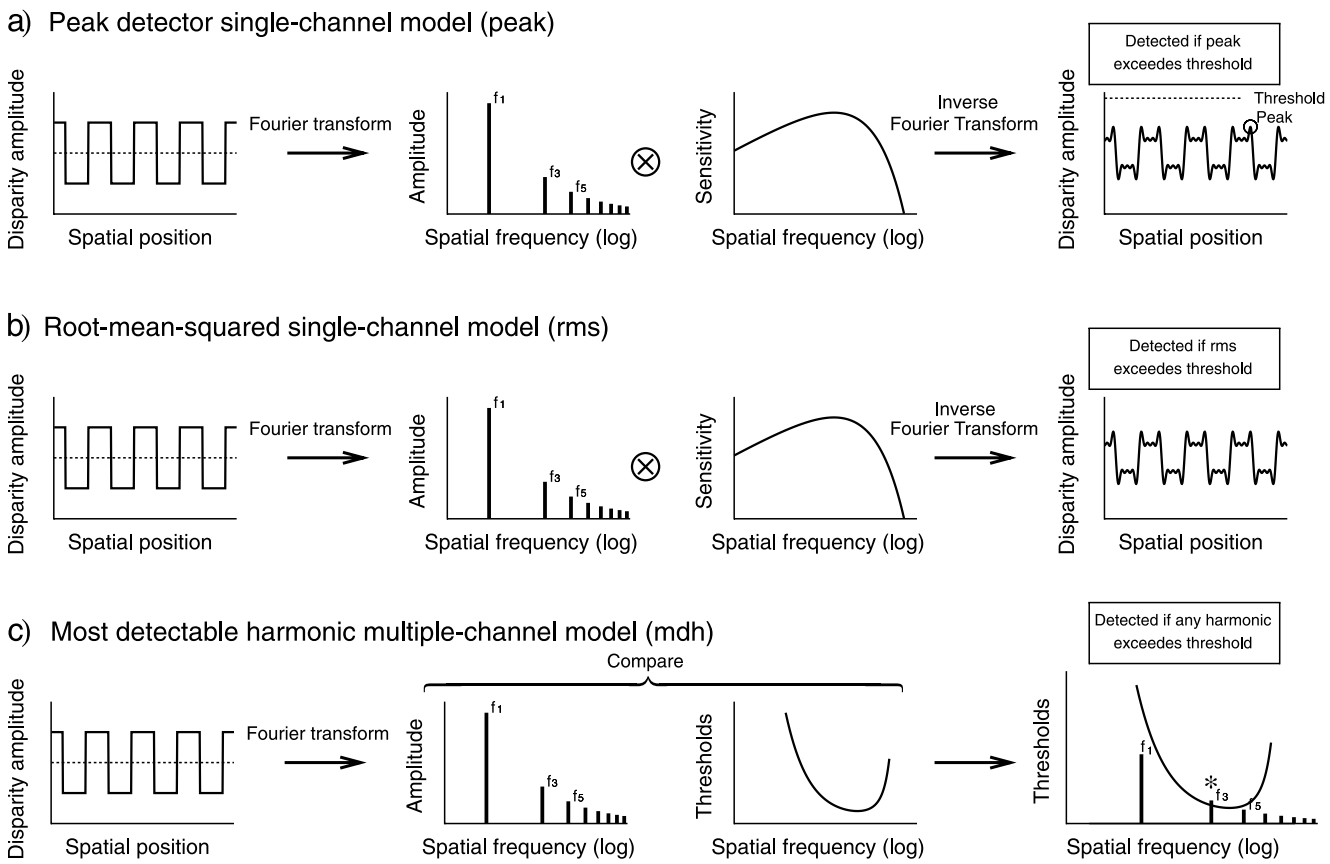

Figure 3. Schematic explaining the principles behind each model. The stimulus waveform is shown on the left of each row. In each case, the first step is to Fourier transform the waveform so as to obtain the amplitude of each component. In the single-channel models, this is then multiplied by the disparity sensitivity function (DSF) and inverse-transformed so as to produce a new waveform, which is the input convolved with a spatial linear operator whose Fourier transform corresponds to DSF. (a) The peak model postulates that the stimulus is detected if the peak amplitude of this filtered waveform exceeds some threshold value; (b) the rms model postulates that it is detected if its rms value exceeds some threshold. (c) The mdh model assumes that the stimulus is analyzed separately within each Fourier harmonic and is detected if any one of its harmonics exceeds the threshold needed to detect that harmonic in isolation.

For a sine wave of peak-to-trough amplitude $A_{\sin}$, the peak of the filtered waveform is

$$P = A_{\sin}\mathrm{DSF}(f_1). \tag{2}$$

Let us say that P is the threshold for detection. Then, $A_{\sin}$ is, by definition, the peak-to-trough disparity threshold for detecting a sine wave of frequency f_1, and therefore $A_{\sin}\mathrm{DSF}(f_1) = 1$. The peak-to-trough disparity threshold for square waves of fundamental frequency f_1 is therefore predicted to be

$$A_{\mathrm{sq}}^{\mathrm{peak}}(f_1) = \frac{1}{\max\left[\frac{4}{\pi}\sum_{n=1,3,5\ldots}^{\infty}\frac{\mathrm{DSF}(nf_1)}{n}\sin(2\pi nf_1 x)\right]}. \tag{3}$$

This prediction is plotted with empty upward triangles in Figures 4 and 5. For comparison, in the lower panels we also plot the ratio of the peak-to-trough threshold amplitude for sine waves to that for square waves:

$$R^{\mathrm{peak}}(f_1) = \frac{A_{\sin}^{\mathrm{peak}}(f_1)}{A_{\mathrm{sq}}^{\mathrm{peak}}(f_1)} = \frac{\max\left[\frac{4}{\pi}\sum_{n=1,3,5\ldots}^{\infty}\frac{\mathrm{DSF}(nf_1)}{n}\sin(2\pi nf_1 x)\right]}{\mathrm{DSF}(f_1)}. \tag{4}$$

Root-mean-squared single-channel model (rms)

Here, the predictions were obtained in the same way as the peak detector model, but we assume that the input waveform is detected when the root-mean-squared (rms) value of the output waveform, not its peak, exceeds some threshold (Kingdom & Keeble, 1996). The rms of the

Downloaded From: http://jov.arvojournals.org/pdfaccess.ashx?url=/data/Journals/JOV/933485/ on 04/12/2016

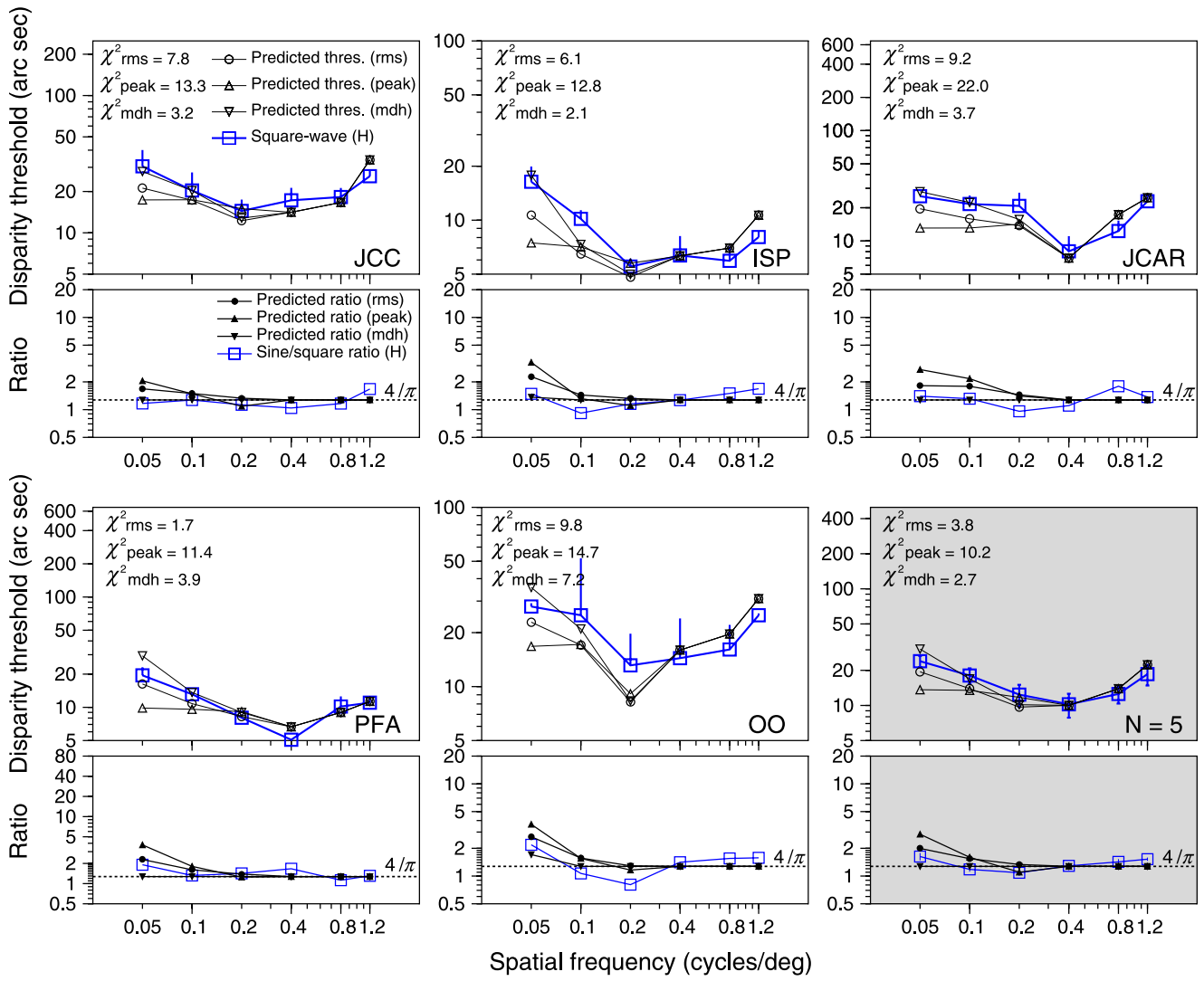

Figure 4. Data and model predictions for horizontally oriented square-wave corrugations. Results are presented in two panels. (Top) Blue squares show the mean of disparity thresholds + *SD* as a function of the spatial frequency of the horizontal square-wave corrugation. Empty circles show the predicted thresholds assuming the rms detection model (rms); upward triangles show the prediction assuming the peak detection model (peak); and downward triangles show the prediction using the most detectable harmonic model (mdh). The goodness of fit between the model thresholds (m) and the data (d) was calculated using $\chi^2 = \Sigma[(d - m)^2/m]$. (Bottom) Blue squares show the ratio between the disparity thresholds of horizontally oriented sine- and square-wave corrugations. Black circles, upward triangles, and downward triangles show the predicted ratio using the predicted disparity thresholds for square-wave corrugations assuming the three models: rms, peak, and mdh, respectively. The dotted line represents the value $4/\pi = 1.2732$. The rightmost panels with gray background show the mean ± *SEM* of the disparity thresholds of all subjects and the predictions of the three models obtained from the mean of disparity thresholds.

output waveform for a square-wave corrugation that peaks at $A_{sq}/2$ is

$$P = A_{sq}\mathrm{rms}\left[\frac{4}{\pi}\sum_{n=1,3,5\ldots}^{\infty}\frac{\mathrm{DSF}(nf_1)}{n}\sin(2\pi nf_1 x)\right], \quad (5)$$

while for a sine wave of peak-to-trough amplitude A_{sin}, it is

$$P = \frac{A_{sin}}{\sqrt{2}}\mathrm{DSF}(f_1). \quad (6)$$

Thus, the predicted peak-to-trough disparity thresholds (empty circles in Figures 4 and 5) for square-wave corrugations are

$$A_{sq}^{rms}(f_1) = \frac{1}{\sqrt{2}\mathrm{rms}\left[\frac{4}{\pi}\sum_{n=1,3,5\ldots}^{\infty}\frac{\mathrm{DSF}(nf_1)}{n}\sin(2\pi nf_1 x)\right]}, \quad (7)$$

Downloaded From: http://jov.arvojournals.org/pdfaccess.ashx?url=/data/Journals/JOV/933485/ on 04/12/2016

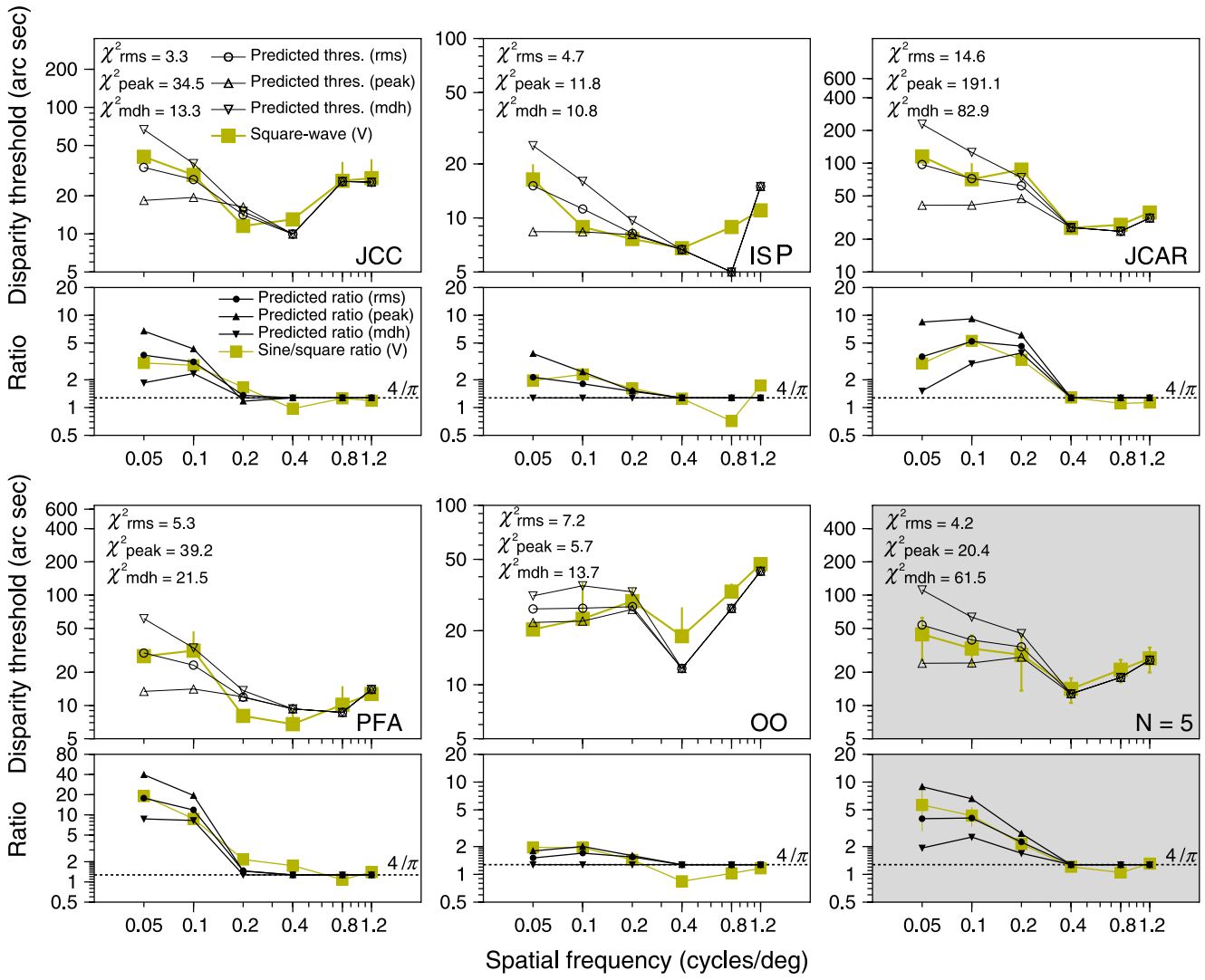

Figure 5. Data and model predictions for vertically oriented square-wave corrugations. Results are presented in two panels. (Top) Brown squares show the mean of disparity thresholds + *SD* as a function of the spatial frequency of the vertical square-wave corrugation. Empty circles show the predicted thresholds assuming the rms detection model (rms); upward triangles show the prediction assuming the peak detection model (peak); and downward triangles show the prediction using the most detectable harmonic model (mdh). (Bottom) Brown squares show the ratio between the disparity thresholds of vertically oriented sine- and square-wave corrugations. Black circles, upward triangles, and downward triangles show the predicted ratio using the predicted disparity thresholds for square-wave corrugations assuming the three models: rms, peak, and mdh, respectively. The rightmost panels with gray background show the mean ± *SEM* of the disparity thresholds of all subjects and the predictions of the three models obtained from the mean of disparity thresholds. Other details as for Figure 4.

and the predicted ratio of sine-wave to square-wave thresholds is

$$R^{\mathrm{rms}}(f_1) = \frac{A_{\mathrm{sin}}^{\mathrm{rms}}(f_1)}{A_{\mathrm{sq}}^{\mathrm{rms}}(f_1)} = \frac{\sqrt{2}\mathrm{rms}\left[\frac{4}{\pi}\sum_{n=1,3,5\ldots}^{\infty}\frac{\mathrm{DSF}(nf_1)}{n}\sin(2\pi nf_1 x)\right]}{\mathrm{DSF}(f_1)}. \quad (8)$$

Most detectable harmonic multiple-channel model (mdh)

This model assumes that the signal is detected by multiple channels. We assume that a waveform is detected whenever any one of its harmonics exceeds the peak-to-trough disparity threshold function (DTF) for that frequency. Thus, a square wave of peak-to-trough amplitude A_{sq} is detected if and only if

$$\frac{4A_{\mathrm{sq}}}{\pi n} \geq \mathrm{DTF}(nf_1) \text{ for any odd } n. \quad (9)$$

Downloaded From: http://jov.arvojournals.org/pdfaccess.ashx?url=/data/Journals/JOV/933485/ on 04/12/2016

At threshold amplitude, the equality holds, and we have

$$\frac{4A_{sq}}{\pi}\max_n \frac{1}{n\mathrm{DTF}(nf_1)} = 1. \quad (10)$$

Rearranging, and expressing in terms of DSF for consistency with the previous expressions, we find that the predicted disparity thresholds (empty downward triangles in Figures 4 and 5) for a square-wave corrugation are

$$A_{sq}^{mdh}(f_1) = \frac{\pi}{4}\min\left[\frac{n}{\mathrm{DSF}(nf_1)}\right], \quad (11)$$

and the predicted ratio of sine-wave to square-wave thresholds is

$$R^{mdh}(f_1) = \frac{A_{sin}^{mdh}(f_1)}{A_{sq}^{mdh}(f_1)} = \frac{4\max(\mathrm{DSF}(nf_1)/n)}{\pi \mathrm{DSF}(f_1)}, \quad (12)$$

where the minimum is taken over odd values of n. If the most detectable harmonic is the fundamental spatial frequency (if $n = 1$), then the ratio will be $4/\pi$.

Model results

Figure 4 shows the predictions of these three linear models for horizontal square-wave corrugations, for each of our 5 subjects individually as well as for the data averaged across subjects. In each case, the blue squares show the psychophysical data, and the black symbols show the predictions of the three models. We show the predictions both as disparity thresholds for the square-wave corrugations (upper panels) and as the ratio of the thresholds for the two corrugations. The goodness of fit between the predicted thresholds and the data is represented by χ^2; the lower the values, the better the fit. Note that the predictions from the three models are identical for spatial frequencies higher that 0.4 cycle/deg, so both here and in the next figure, the thresholds measured at low spatial frequencies are critical for distinguishing between the models.

We consider first the mdh model (∇ symbols). Since a square wave's higher harmonics have much lower amplitude than its fundamental, and the disparity sensitivity function measured with horizontal sine corrugations is relatively shallow, the fundamental is in most cases the first component to rise above threshold. Thus, the mdh model usually predicts that the ratio of disparity threshold with horizontal sine waves to that with horizontal square waves is $4/\pi = 1.273$, the amplitude ratio of their fundamental components. This model predicts experimental thresholds well in all subjects.

The rms model ($\circ$) produces very similar predictions to the mdh. The mean of the χ^2_{rms} values over the five subjects is 6.92, slightly worse than the mean of 4.02 for χ^2_{mdh}. In almost all cases, the peak model (Δ) is far worse at predicting the experimental data.

We conclude that both the rms and mdh models are adequate to account for detection thresholds for square-wave horizontally oriented disparity corrugations. Thus, the data so far do not enable us to distinguish clearly between single-channel and multi-channel models for disparity detection.

Figure 5 shows the results with the predictions for vertical square-wave corrugations. The most noticeable difference in the data, compared to horizontal corrugations, is the high ratio of sine/square thresholds, well in excess of $4/\pi$ at low frequencies. The mdh model (∇) does go some way toward capturing this. For vertically oriented corrugations, the threshold ratio predicted by the mdh model can exceed the classic value of $4/\pi$. This interesting effect is due to the very steep increase in threshold at low frequencies, which does not occur for horizontally oriented disparity corrugations, nor in the luminance domain. As frequency increases from 0.05 cycle/deg, disparity thresholds for sine corrugations fall faster than the $1/n$ decay in harmonics of the square wave. This means that it is possible for the square-wave's fifth harmonic at $5f_1$, for example, to be above threshold, while its fundamental at f_1 is still undetectable. Thus, the mdh model produces threshold ratios approaching 5 in some subjects. However, its threshold ratios are still substantially smaller than those observed experimentally: subjects do much better on the square-wave corrugations than predicted by this model.

The peak model (Δ), in contrast, predicts that subjects do too well on the square-wave corrugations; its predicted thresholds are consistently too low at the lowest spatial frequencies. However, the rms model ($\circ$) shows the best fit of all three models, capturing the data remarkably well for all subjects and frequencies, without any free parameters. Since this model also accounted well for the horizontal data (Figure 4), as far as our data are concerned, a single linear channel could underlie the detection of both horizontally and vertically oriented square-wave corrugations.

Discussion

We began this study by replicating some well-known results concerning disparity corrugations. Like previous workers, we find a strong stereo anisotropy affecting sinusoidal disparity corrugations of spatial frequencies below 0.4 cycle/deg, whereby the threshold for a vertically oriented corrugation is higher than for the same corrugation oriented horizontally (see Figure 4; Bradshaw et al., 2006; Bradshaw & Rogers, 1999). We also reproduced the U-shape of the disparity thresholds and the maximum

Downloaded From: http://jov.arvojournals.org/pdfaccess.ashx?url=/data/Journals/JOV/933485/ on 04/12/2016

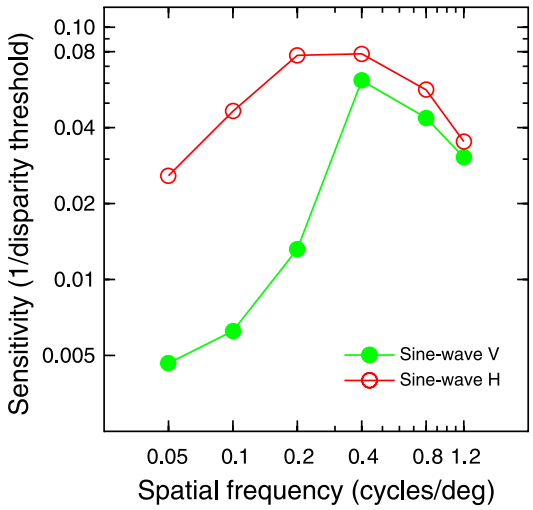

Figure 6. Disparity sensitivity functions (DSFs) from population-average data (Figure 2, gray panels). The DSFs were obtained taking the inverse of the average disparity thresholds. Red circles, DSF for horizontally oriented sine-wave corrugations. Green dots, DSF for vertically oriented sine-wave corrugations.

sensitivity about 0.4 cycle/deg (Bradshaw & Rogers, 1999; Rogers & Graham, 1982; van der Willigen et al., 2010).

Interestingly, we have shown that the disparity thresholds for square-wave corrugations do not show this strong anisotropy at low spatial frequencies. Although the disparity thresholds for vertically oriented square corrugations were in general higher than those obtained with horizontally oriented corrugations, this difference was independent of the spatial frequency.

We have examined three different linear models (peak, rms, and mdh) imported from the domain of luminance and texture domain (Campbell & Robson, 1968; Kingdom & Keeble, 1996) to see whether they can predict thresholds for square-wave gratings from the values measured for sine waves. These differ in the number of disparity channels they postulate, using "channels" in the sense of "linearly operating independent mechanisms selectively sensitive to limited ranges of spatial frequencies" (Campbell & Robson, 1968). The peak and rms models are both based on a single, broadly tuned channel, while the "most detectable harmonic" or mdh model goes to the other extreme and assumes each harmonic is detected by a separate channel. The peak model could not explain the results well for either horizontally or vertically oriented gratings and can therefore be rejected.

For horizontally oriented corrugations, both the single-channel rms and the multi-channel mdh models explained our data equally well. Both models successfully account for the weak orientation anisotropy observed for horizontal vs. vertical square-wave corrugations at all frequencies, despite the strong anisotropy observed for horizontal vs. vertical sine-wave corrugations at low frequencies. Thus, our data provide little reason to choose between the rms and mdh models. However, much previous evidence (Cobo-Lewis & Yeh, 1994; Lee & Rogers, 1997; Tyler, 1975; Schumer & Ganz, 1979) indicates that there are multiple disparity spatial frequency channels, just as in the luminance domain, albeit more broadly tuned. Thus, for horizontally oriented corrugations, the multi-channel mdh model is most consistent with both the present data and the previous literature.

For vertically oriented corrugations, only the single-channel rms model (Kingdom & Keeble, 1996) could explain our results. All previous investigations of disparity channels have used horizontally oriented gratings, so there is no evidence for multiple disparity spatial frequency channels tuned to vertical orientations. We therefore suggest that vertically oriented disparity modulations may be detected by a single channel. This idea is supported by Figure 6, which shows the disparity sensitivity functions we have obtained for horizontally and vertically oriented sinusoidal disparity corrugations. The peak sensitivity is similar, but the vertical sensitivity function is much narrower. It has a full-width half-amplitude bandwidth of 2.1 octaves, comparable with previous estimates for the bandwidth of individual channels tuned to horizontally oriented disparity modulations (2–3 octaves, Schumer & Ganz, 1979). In contrast, the horizontal sensitivity function has a bandwidth of 3.8 octaves. We suggest that this may be because the vertical sensitivity function represents a single disparity channel, whereas the horizontal sensitivity function is the envelope of two or more such channels. This difference in channel number may be the underlying reason for the famous stereo anisotropy.

Acknowledgments

Some of the findings described have been reported previously in the European Conference on Visual Perception 2009 (Serrano-Pedraza & Read, 2009a). We thank Vicente Sierra-Vázquez for helpful comments on the manuscript. This work was supported by the Royal Society (University Research Fellowship UF041260 to JCAR) and Medical Research Council (New Investigator Award 80154).

Commercial relationships: none.
Corresponding author: Ignacio Serrano-Pedraza.
Email: i.s.pedraza@ncl.ac.uk.
Address: Henry Wellcome Building, Framlington Place, Newcastle upon Tyne, NE2 4HH, UK.

References

Anderson, A. J. (2003). Utility of a dynamic termination criterion in the ZEST adaptive threshold method. *Vision Research, 43,* 165–170.

Downloaded From: http://jov.arvojournals.org/pdfaccess.ashx?url=/data/Journals/JOV/933485/ on 04/12/2016

Bradshaw, M. F., Hibbard, P. B., Parton, A. D., Rose, D., & Langley, K. (2006). Surface orientation, modulation frequency and the detection and perception of depth defined by binocular disparity and motion parallax. *Vision Research, 46,* 2636–2644.

Bradshaw, M. F., & Rogers, B. J. (1999). Sensitivity to horizontal and vertical corrugations defined by binocular disparity. *Vision Research, 39,* 3049–3056.

Brainard, D. H. (1997). The psychophysics toolbox. *Spatial Vision, 10,* 433–436.

Campbell, F. W., & Robson, J. G. (1968). Application of Fourier analysis to the visibility of gratings. *The Journal of Physiology, 197,* 551–566.

Cobo-Lewis, A. B., & Yeh, Y. (1994). Selectivity of cyclopean masking for the spatial frequency of binocular disparity modulation. *Vision Research, 34,* 607–620.

Emerson, P. L. (1986). Observations on maximum likelihood and Bayesian methods of forced-choice sequential threshold estimation. *Perception & Psychophysics, 39,* 151–153.

García-Pérez, M. A. (1998). Forced-choice staircases with fixed steps sizes: Asymptotic and small-sample properties. *Vision Research, 38,* 1861–1881.

Kingdom, F. A. A., & Keeble, D. R. T. (1996). A linear systems approach to the detection of both abrupt and smooth spatial variations in orientation-defined textures. *Vision Research, 36,* 409–420.

King-Smith, P. E., Grigsby, S. S., Vingrys, A. J., Benes, S. C., & Supowit, A. (1994). Efficient and unbiased modifications of the QUEST threshold method: Theory, simulations, experimental evaluation and practical implementation. *Vision Research, 34,* 885–912.

Lee, B., & Rogers, B. J. (1997). Disparity modulation sensitivity for narrow-band-filtered stereograms. *Vision Research, 37,* 1769–1777.

Pelli, D. G. (1997). The VideoToolbox software for visual psychophysics: Transforming numbers into movies. *Spatial Vision, 10,* 437–442.

Pentland, A. (1980). Maximum likelihood estimation: The best PEST. *Perception & Psychophysics, 28,* 377–379.

Rogers, B. J., & Graham, M. E. (1982). Similarities between motion parallax and stereopsis in human depth perception. *Vision Research, 22,* 261–270.

Schumer, R., & Ganz, L. (1979). Independent stereoscopic channels for different extents of spatial pooling. *Vision Research, 19,* 1303–1314.

Serrano-Pedraza, I., & Read, J. C. A. (2009a). Horizontal/vertical anisotropy in sensitivity to relative disparity depends on stimulus depth structure. *Perception, 38,* 155.

Serrano-Pedraza, I., & Read, J. C. A. (2009b). Stereo vision requires an explicit encoding of vertical disparity. *Journal of Vision, 9*(4):3, http://www.journalofvision.org/content/9/4/3, doi:10.1167/9.4.3. [PubMed] [Article]

Treutwein, B. (1995). Adaptive psychophysical procedures. *Vision Research, 35,* 2503–2522.

Tyler, C. W. (1974). Depth perception in disparity gratings. *Nature, 251,* 140–142.

Tyler, C. W. (1975). Stereoscopic tilt and size aftereffects. *Perception, 4,* 187–192.

Tyler, C. W. (1991). Cyclopean vision. In D. Regan (Ed.), *Vision and visual dysfunction, binocular vision* (vol. 9, pp. 38–74). London: Macmillan.

Tyler, C. W., & Raibert, M. (1975). Generation of random-dot stereogratings. *Behavior Research Methods and Instrumentation, 7,* 37–41.

van der Willigen, R. F., Harmening, W. M., Vossen, S., & Wagner, H. (2010). Disparity sensitivity in man and owl: Psychophysical evidence for equivalent perception of shape-from-stereo. *Journal of Vision, 10*(1):10, http://www.journalofvision.org/content/10/1/10, doi:10.1167/10.1.10. [PubMed] [Article]

Downloaded From: http://jov.arvojournals.org/pdfaccess.ashx?url=/data/Journals/JOV/933485/ on 04/12/2016